Cell Sorting

DOI: 10.1002/ange.201409376

Nanoparticle-Mediated Binning and Profiling of Heterogeneous Circulating Tumor Cell Subpopulations**

*Reza M. Mohamadi, Justin D. Besant, Adam Mepham, Brenda Green, Laili Mahmoudian, Thaddeus Gibbs, Ivaylo Ivanov, Anahita Malvea, Jessica Stojcic, Alison L. Allan, Lori E. Lowes, Edward H. Sargent, Robert K. Nam, and Shana O. Kelley**

Abstract: *The analysis of circulating tumor cells (CTCs) is an important capability that may lead to new approaches for cancer management. CTC capture devices developed to date isolate a bulk population of CTCs and do not differentiate subpopulations that may have varying phenotypes with different levels of clinical relevance. Here, we present a new device for CTC spatial sorting and profiling that sequesters blood-borne tumor cells with different phenotypes into discrete spatial bins. Validation data are presented showing that cancer cell lines with varying surface expression generate different binning profiles within the device. Working with patient blood samples, we obtain profiles that elucidate the heterogeneity of CTC populations present in cancer patients and also report on the status of CTCs within the epithelial-to-mesenchymal transition (EMT).*

Circulating tumor cells (CTC) are shed into the vasculature from primary tumors, and have been shown to contribute to the formation of metastases in model systems.[1,2] Several studies suggest that CTC counts in the blood of cancer patients can be correlated with aggressive disease and poor prognosis.[3] Since individual tumors can be highly heterogeneous and contain many cellular subpopulations,[4,5] an individual patient's CTCs may be heterogeneous, containing subpopulations having varying relevance to the development of metastatic disease.[6–8] Therefore, rather than simply counting circulating tumor cells, it is important to monitor the distribution of CTC populations and sort them according to surface marker expression to gain more insight into the clinical relevance of blood-borne CTC.

The development of high-performance fluidic devices for CTC capture and analysis is a rapidly advancing field.[9] Powerful approaches based on droplet aliquoting,[10] affinity capture and readout,[11–20] differential adhesion,[21] negative selection,[21] size-based separation,[22,23] and even combinations of size- and affinity-based capture[24] have been reported, and these devices have permitted more sensitive measurements of CTC count. However, many existing devices seek simply to isolate the set of all CTCs in a sample, and do not separate them into distinct subpopulations.

Our basic approach to binning CTC subpopulations relies on the tagging of cells with magnetic nanoparticles directed toward a surface marker (Figure 1 A). This approach was initially developed using the epithelial marker EpCAM as a target. One source of potential heterogeneity in CTCs is related to the fact that these cells may undergo the epithelial–mesenchymal transition (EMT),[22] in which epithelial markers are gradually lost. Many studies have shown that changes in EpCAM expression occur in patient CTCs,[3] and the extent of EpCAM loss has been linked with the metastatic potential of CTCs.[8] Furthermore, the appearance of CTCs with lowered levels of epithelial markers is a predictor of cancer recurrence.[7] It is therefore critically important to develop straightforward methods for the determination of the EpCAM profile for circulating tumor cells. While single-cell methods can potentially provide a means to profile expression levels in individual CTCs, they are destructive (i.e., they result in the loss of the cell), and they are challenging to implement and prone to artifacts from the presence of contaminating cells.

By tagging cells with EpCAM-targeted nanoparticles, we labeled CTCs to differing extents depending on their phenotype. This targeting strategy was combined with an approach to fluidic capture that allows CTCs with different numbers of nanoparticles to be trapped in different compartments of a fluidic chip (Figure 1 B,C). Whereas prior reports have used anti-EpCAM-labeled particles to trap CTCs,[18–20] none featured the compartmentalization included in this approach.

Nanoparticle-tagged cells can be captured within a fluidic device when the retaining magnetic force overcomes the drag force that opposes capture. However, the low magnetic

[*] Dr. R. M. Mohamadi, Dr. L. Mahmoudian, T. Gibbs, Dr. I. Ivanov, A. Malvea, Prof. S. O. Kelley
Leslie Dan Faculty of Pharmacy
University of Toronto, Toronto, ON (Canada)
J. D. Besant, A. Mepham, B. Green, Prof. S. O. Kelley
Institute of Biomaterials and Biomedical Engineering
University of Toronto, Toronto, ON (Canada)
J. Stojcic, R. K. Nam
Sunnybrook Research Institute, Toronto, ON (Canada)
A. L. Allan, L. E. Lowes
London Health Sciences Centre, London, ON (Canada)
Prof. E. H. Sargent
Department of Electrical and Computer Engineering
University of Toronto, Toronto, ON (Canada)
Prof. S. O. Kelley
Department of Biochemistry
University of Toronto, Toronto, ON (Canada)
E-mail: shana.kelley@utoronto.ca

[**] S.O.K, E.H.S., and R.K.N. acknowledge the Canadian Institutes of Health Research and the Ontario Research Fund. The cancer patients and healthy individuals who donated samples are also gratefully acknowledged.

Supporting information for this article is available on the WWW under http://dx.doi.org/10.1002/anie.201409376.

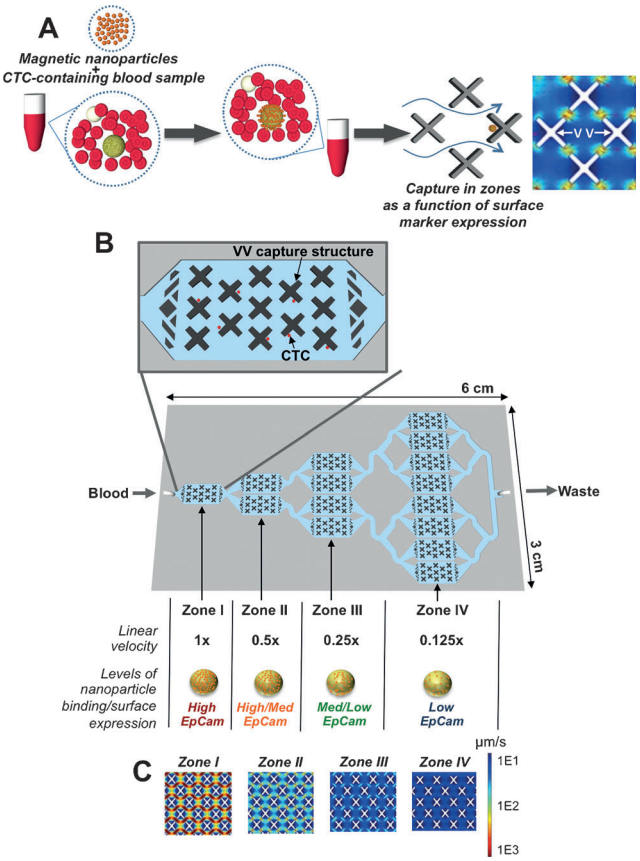

Figure 1. Design of a device for surface-expression-guided binning of heterogeneous circulating tumor cells. A) CTCs are tagged with magnetic nanoparticles functionalized with an antibody against the surface marker EpCAM. Labeled CTCs are magnetically captured in the local velocity valleys (VVs) generated by the capture structures (rightmost graphic shows low flow regions in blue, high flow in red). B) A multizone velocity valley device that features four different regions with different linear velocities (1×, 0.5×, 0.25×, and 0.125×). High EpCAM cells will be trapped in zone I, with cells with medium to low EpCAM levels being trapped in later zones. C) Flow profiles for zones I–IV showing the decrease in linear velocity in the different zones.

susceptibility of nanoparticles leads to a low magnetic force that is easily overcome by the drag force at very low flow rates (~0.05 mL h^{-1}; see the Supporting Information (SI) Figure S1). We hypothesized that, if microfabricated structures were introduced within a fluidic device that would create localized pockets of low flow velocity (velocity valleys, VVs), regions would be created that strongly favored the accumulation of the targeted cells (Figure 1A). These structures could then be introduced into fluidic zones with varying volumes that would alter the linear velocity of the flowing solution (Figure 1A). This would allow CTCs with a high level of labeling and higher magnetic susceptibility to be trapped in zones in which the drag force is higher, whereas less highly labeled cells would continue moving and only become trapped once they entered a zone with lower linear velocity.

We tested the capture efficiency of X-shaped velocity valleys first in a single-zone chip (Figure 2A) to benchmark the performance of the fluidic approach (see SI for all experimental protocols). Target cells were mixed with 50 nm magnetic particles coated with anti-EpCAM in buffered solution. The sample was then pumped through a VV chip and washed. The efficiency of capture was measured by staining nucleated cells with DAPI, and counting cells with microscopy.

Using this approach, we were able to visualize captured cells in the VV structures. As shown in Figure 2B, VCaP cells (prostate cancer cells that overexpress EpCAM) were captured with high efficiency in the VV chip. Control U937 cells that do not overexpress EpCAM were not captured (Figure 2C). Simulations of the role of the VVs in facilitating cell capture were conducted, and it was determined that X-shaped structures were optimal for high efficiency capture (Figure S1). Trials conducted with differently shaped microstructures (Figure 2D) were consistent with the simulation.

To assess the performance of the VV approach in a complex sample, we evaluated the cell capture efficiency in whole blood (Figure 2E and F). We challenged the system with blood samples spiked with different numbers of VCaP cells and developed an immunostaining-based approach to specific cancer cell identification. The captured cells were fixed and immunostained to distinguish nucleated white blood cells (WBC) from target cells. Cancer cells were distinguished by a triple stain for cytokeratin (CK^+), a nuclear stain ($DAPI^+$), and by confirmation that they were lacking any staining for CD45 ($CD45^-$). No more than 200 white blood cells were typically observed in the fluidic device, indicating that large gains in enrichment could be made (see Table S3).

We compared directly the performance of the velocity valley approach with the gold standard, FDA-cleared CellSearch assay (Figure 2E). Spiked blood samples containing 2 to 25 VCap cells per milliliter were prepared, and analyzed using CellSearch and the VV chip coupled with standard protocols for identifying CTCs by immunostaining.[23] Two unspiked samples lacking VCap cells were tested using the VV chip and CellSearch, and no cancer cells were detected. For the spiked samples, the VV approach outperformed CellSearch at every concentration tested. Importantly, cells captured in the VV device can be selectively recovered and cultured (see SI, Figure S6).

A unique advantage of using nanoparticles for cell capture relates to the large number of binding events that contribute to specific capture. Thousands of nanoparticles can bind to a cell expressing a target surface marker, and the exact number of particles depends on expression levels. We therefore posited that cells could be sorted and binned—as a function of their quantitative level of target surface marker expression—into different compartments of a velocity valley chip where each stage was designed to have a different linear velocity. Such a capability would allow heterogeneous populations of CTCs to be separated and analyzed.

A velocity valley chip was fabricated that contained four sorting zones (Figure 1B). The first compartment within the chip was designed to have a high linear velocity that would only retain cells with a high nanoparticle population. The following three zones had velocities that decreased stepwise

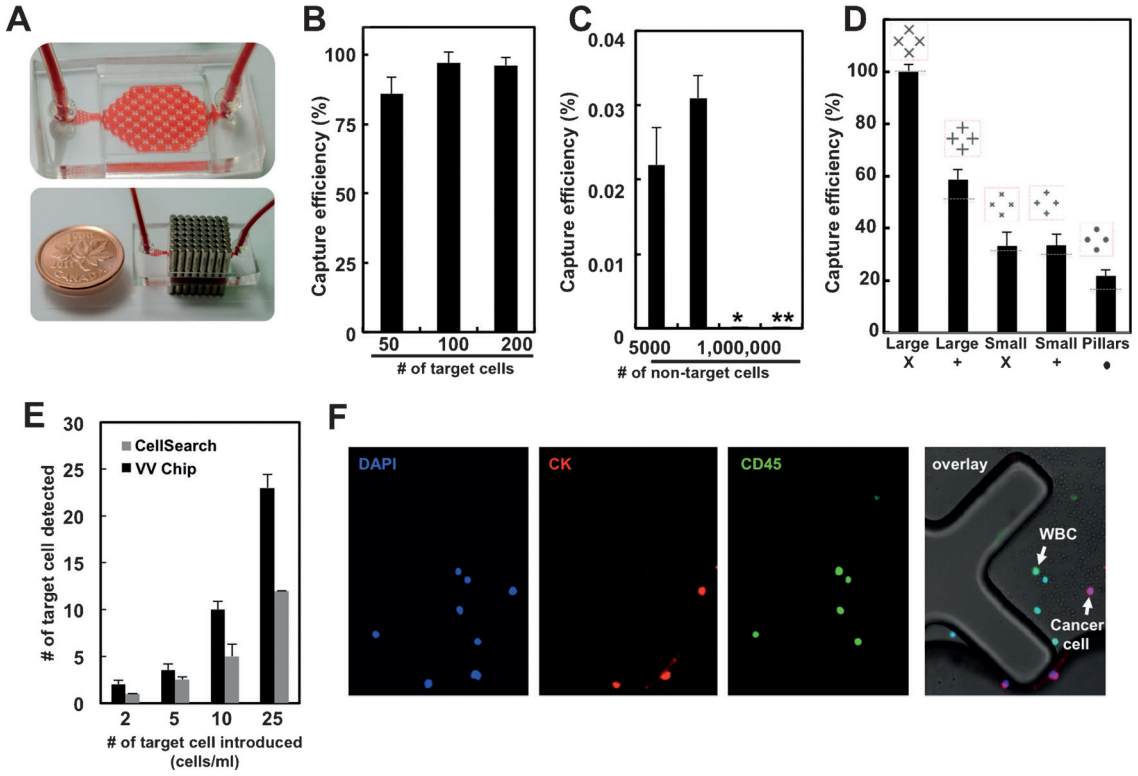

Figure 2. Validation of the velocity valley (VV) capture approach. A) A single-zone device for validation of the velocity-valley-mediated capture approach. The device is loaded with whole blood and an array of magnets is applied to trap cells with bound nanoparticles. B) Capture efficiency as a function of the number of target cells (VCaP) and C) non-target cells (U937) in buffer solution. Cells were stained with DAPI and counted. Nonspecific capture without nanoparticles (*) or a magnetic field (**) is negligible. Error bars show standard deviations, $n \geq 3$. D) The effect of trapping structure geometry on capture efficiency of VCaP cells. In simulations (Figure S1) and experimental trials, large X-shaped structures were most efficient at capturing cells. The agreement between the capture efficiencies predicted by the model (gray lines) and the experimental data validates the mechanism of capture as relating to the formation of velocity valleys within the fluidic chip. E) Head-to-head comparison of the VV chip with CellSearch. Samples analyzed were VCaP cells spiked into whole blood. Error bars show standard deviations, $n \geq 3$. Control samples ($n = 2$) were collected from healthy donors and no positive cells were detected. F) Immunostaining-based analysis of whole blood spiked with VCaP cells. Captured cells were identified using a triple stain of DAPI, anti-CK, and anti-CD45. It is noteworthy that although cells are trapped in the low flow regions of the VVs (Supporting Video S2), the release of the magnetic field during immunostaining allows the cells to move slightly. The trials shown in this Figure were conducted with a flow rate of $2\,mL\,h^{-1}$, but flow rates up to $40\,mL\,h^{-1}$ can be used without a decrease in capture efficiency (Figure S2 B).

by a factor of two. The target linear velocities for the different compartments of the device were determined by taking into consideration the range of expression levels for EpCAM in cancer cells. Previous studies have quantitated EpCAM levels and have shown that levels vary from 1×10^4 molecules per cell to 1×10^7 molecules per cell.[25] We designed our chip to target the lower range of expression to resolve populations of CTCs with lowered expression of EpCAM (see Figure S4, SI).

To validate the performance of this chip, three cell lines that were known and validated using flow cytometry (Figure 3 A) to have different EpCAM expression levels[22] were introduced into the chip, and immunofluorescence was used to count the cells that were captured in each zone. The three different cell lines with different levels of EpCAM showed a distinctly different, and highly reproducible pattern of distribution within the chip (Figure 3 B). VCap cells, which have a high level of EpCAM expression, were mainly found in zone I, as the high number of nanoparticles bound to their surfaces allowed them to be retained despite a high flow velocity. SKBR3 cells, which have a ca. 10-fold lower level of EpCAM expression, were found predominantly in zone I and II. MDA-MB-231 cells, which have EpCAM levels reduced by another 10-fold, were found mainly in zones III and IV. These results indicate that cells can be sorted according to expression levels of a surface marker, and that even cells with very low EpCAM expression can be captured. The data shown in Figure 3 were collected from a series of independent trials, and the strong statistical significance of the data indicates that the number of cells detected in each zone from trial-to-trial was subject to minimal drift.

We analyzed a set of patient samples using the multizone chip and immunostaining to determine if this approach would be effective with clinical samples, and to determine whether different patients would exhibit different subpopulation profiles. We first processed a single sample collected from a patient with prostate cancer in two identical chips to first determine whether the data obtained from patient samples was reproducible (Figure 4 A). The patient sample was split, processed, and analyzed (Figure 4 B) using two independent sorting chips; freshly collected blood was introduced into the

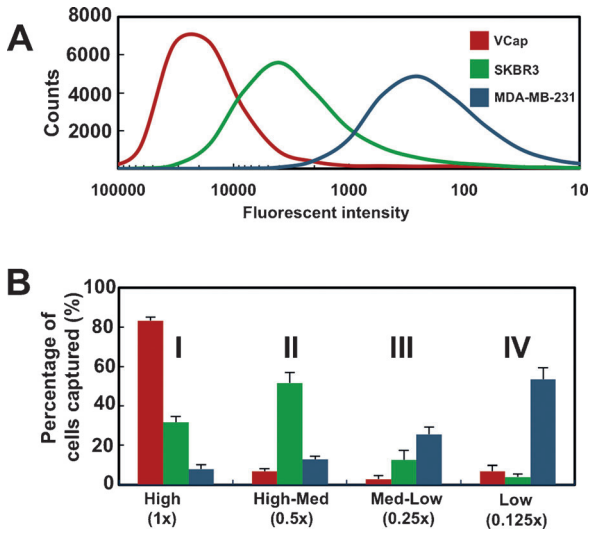

Figure 3. Cells with different surface marker expression levels can be binned in a multizone device. A) Expression of EpCAM on three cell lines tested using fluorescently labeled anti-EpCAM and flow cytometry. B) Distribution of Vcap (red), SKBR3 (green), and MDA-MB-231 (blue) cells in the multizone device. Cell lines with different EpCAM expression levels were captured in different zones of the device shown in Figure 1 B, demonstrating that binning of cells with different surface expression profiles is feasible and reproducible.

device with no preprocessing except for the addition of magnetic nanoparticles. This analysis determined that a single sample yielded a consistent profile in the two devices, even when very small numbers of cells were discovered.

A set of prostate cancer patient samples were analyzed using this approach (Figure 4 C), and many different types of profiles were obtained. Many samples exhibited profiles with CTCs appearing in different capture zones, consistent with a high degree of heterogeneity existing within a single patient's CTCs. Some samples exhibited the highest number of cells in zone I, whereas others had the highest levels in zone II, III, or IV. The CTCs detected within some patient samples appeared to retain significant EpCAM levels and epithelial character (e.g., P2 and P3), whereas other samples had many more cells in zones III and IV (e.g., P5 and P15), indicating low EpCAM expression and a loss of epithelial character. Confirmation of decreasing EpCAM levels in higher zones was confirmed by reverse-transciption and PCR (Table S5). The different profiles observed likely report on whether CTCs in individual patients have undergone EMT, which has previously been shown to correlate with disease aggressiveness.[7] All of the patients tested were diagnosed identically with localized prostate cancer; the varied CTC profiles may indicate that molecular-level differences exist in the patients' tumors.

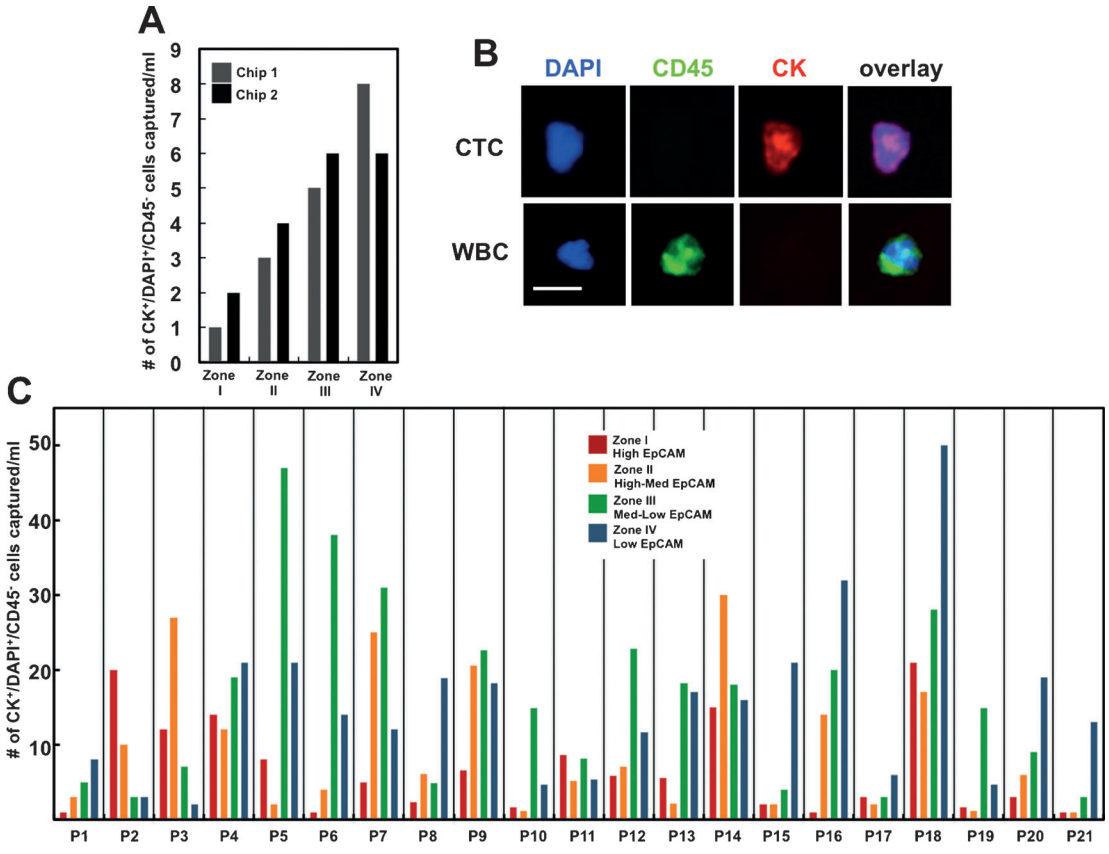

Figure 4. Patient CTCs with different surface marker expression levels can be binned in a multizone device. A) Reproducibility of binning patterns. Two runs using the same patient blood sample produced a similar pattern of CTC capture in the multizone VV chip. B) Identification and counting of CTCs based on immunostaining. Cells were fixed and stained with antibodies against CD45 and cytokeratin, and the DAPI nuclear stain. Cells that were positive for CK and DAPI, but negative for CD45 were identified as CTCs. C) Surface-marker-guided binning profiles for prostate cancer patient samples reported on a CTC mL^{-1} basis. Cells were counted if they were $CK^+/DAPI^+/CD45^-$ as shown in (B). Control samples ($n=3$) were collected from healthy donors and no positive cells were detected.

It is noteworthy that the approach reported is highly versatile and can use a variety of surface markers for CTC binning and profiling. For example, we tested MUC1 and HER2 as target capture antigens and successfully sorted cells with nanoparticles displaying antibodies against these factors (Figure S5). Therefore, the capabilities of the device go well beyond sorting based on EpCAM levels.

In summary, we report a new means of analyzing CTCs and describe a solution that allows the characterization of specific subpopulations found in patient samples. Using a simple fluidic device that bins cells into compartments according to their levels of an epithelial marker, discrete CTC subpopulations can be spatially sorted. The approach provides a powerful means to study EMT in patient CTCs, and the sensitivity of the approach exceeds that obtained with the gold standard CellSearch method. The highly tunable nature of this approach permits the construction of a multizone chip that uses regions of varying linear velocity to trap cells with different levels of antigen-targeted nanoparticles.

Received: September 22, 2014
Revised: October 21, 2014
Published online: November 5, 2014

Keywords: cancer cell analysis · cell sorting · magnetic nanoparticles · microfluidics · tumor cells

[1] C. L. Chaffer, R. A. Weinberg, *Science* **2011**, *331*, 1559 – 1564.
[2] K. Pantel, C. Alix-Panabieres, S. Riethdorf, *Nat. Rev. Clin. Oncol.* **2009**, *6*, 339 – 351.
[3] K. Pantel, S. Riethdorf, *Nat. Rev. Clin. Oncol.* **2009**, *6*, 190 – 191.
[4] P. L. Bedard, A. R. Hansen, M. J. Ratain, L. L. Siu, *Nature* **2013**, *501*, 355 – 364.
[5] C. E. Meacham, S. J. Morrison, *Nature* **2013**, *501*, 328 – 337.
[6] I. Baccelli, et al., *Nat. Biotechnol.* **2013**, *31*, 539 – 544.
[7] M. Yu, et al., *Science* **2013**, *339*, 580 – 584.
[8] L. Zhang, L. D. Ridgway, M. D. Wetzel, J. Ngo, W. Yin, D. Kumar, J. C. Goodman, M. D. Groves, D. Marchetti, *Sci. Transl. Med.* **2013**, *5*, 180ra48.
[9] C. Alix-Panabières, K. Pantel, *Lab Chip* **2014**, *14*, 57 – 62.
[10] P. G. Schiro, M. Zhao, J. S. Kuo, K. M. Koehler, D. E. Sabath, D. T. Chiu, *Angew. Chem. Int. Ed.* **2012**, *51*, 4618 – 4622; *Angew. Chem.* **2012**, *124*, 4696 – 4700.
[11] J. D. Adams, U. Kim, H. T. Soh, *Proc. Natl. Acad. Sci. USA* **2008**, *105*, 18165 – 18170.
[12] E. Ozkumur, et al., *Sci. Transl. Med.* **2013**, *5*, 179ra47.
[13] J. W. Kamande, et al., *Anal. Chem.* **2013**, *85*, 9092 – 9100.
[14] M. Zhao, P. G. Schiro, J. S. Kuo, K. M. Koehler, D. E. Sabath, V. Popov, Q. Feng, D. T. Chiu, *Anal. Chem.* **2013**, *85*, 2465 – 2471.
[15] H. J. Yoon, et al., *Nat. Nanotechnol.* **2013**, *8*, 735 – 741.
[16] D. Issadore, J. Chung, H. Shao, M. Liong, A. A. Ghazani, C. M. Castro, R. Weissleder, H. Lee, *Sci. Transl. Med.* **2012**, *4*, 141ra92.
[17] S. Wang, et al., *Angew. Chem. Int. Ed.* **2011**, *50*, 3084 – 3088; *Angew. Chem.* **2011**, *123*, 3140 – 3144.
[18] K. Hoshino, Y. Y. Huang, N. Lane, M. Huebschman, J. W. Uhr, E. P. Frenkel, X. Zhang, *Lab Chip* **2011**, *11*, 3449 – 3457.
[19] J. H. Kang, S. Krause, H. Tobin, A. Mammoto, M. Kanapathipillai, D. E. Ingber, *Lab Chip* **2012**, *12*, 2175 – 2181.
[20] S. Kim, S. I. Han, M. J. Park, C. W. Jeon, Y. D. Joo, I. H. Choi, K. H. Han, *Anal. Chem.* **2013**, *85*, 2779 – 2786.
[21] B. P. Casavant, et al., *Methods* **2013**, *64*, 137 – 143.
[22] F. A. Coumans, G. van Dalum, M. Beck, L. W. Terstappen, *PLoS One* **2013**, *8*, e61774.
[23] D. R. Parkinson, et al., *J. Transl. Med.* **2012**, *10*, 138.
[24] H. J. Lee, et al., *Angew. Chem. Int. Ed.* **2013**, *52*, 8337 – 8340; *Angew. Chem.* **2013**, *125*, 8495 – 8498.
[25] N. Prang, et al., *Br. J. Cancer* **2005**, *92*, 342 – 349.

